Flame Spread in Low-Speed Forced Flows: Ground- and Space-Based Experiments

Shuangfeng Wang and Feng Zhu

Abstract Flame spread across solid materials in low-velocity flow regime is of fundamental interest and practical importance, whereas experiments for this type of combustion have been a challenge. The present article introduces recent progress of this research field in the light of the flame spread experiments that have been performed at the Key Laboratory of Microgravity, CAS. The experimental methods employed to offer a slow convective flow include the narrow channel apparatus in normal gravity, ground-based microgravity free drops, and orbital space flights. The highlighted topics involve the confinement effects on flame spread, concurrent flame behaviors near the quenching limit, flame spread and extinction over thick solids in opposed and concurrent flows, and dynamics of spreading flame over thick solids in step-changed flow.

Keywords Flame spread · Low-velocity flow · Microgravity · SJ-10 Satellite of China · Narrow channel apparatus

1 Introduction

Flame spread over the surface of a solid combustible material constitutes a unique configuration of propagating diffusion flame combustion, and is generally considered as a significant model of real life fire processes. Compared with conventional homogeneous diffusion flames in gases, the flame spreading over solids is different in that the fuel is originally in condensed phase and the pyrolysis process of the solid is needed to generate fuel vapor. Thus the flame spread phenomena involve inherently complex interaction of heat and mass transport processes, and the

S. Wang (✉) · F. Zhu
Key Laboratory of Microgravity (National Microgravity Laboratory), Institute of Mechanics, Chinese Academy of Sciences, Beijing 100190, China
e-mail: sfwang@imech.ac.cn

School of Engineering Science, University of Chinese Academy of Sciences, Beijing 100049, China

W. R. Hu and Q. Kang (eds.), *Physical Science Under Microgravity: Experiments on Board the SJ-10 Recoverable Satellite*, Research for Development,
https://doi.org/10.1007/978-981-13-1340-0_10

chemical reaction in both gaseous and condensed phases. In addition, as the flame spreads across the solid surface, heat transfer takes place at least in the parallel and perpendicular directions simultaneously, i.e., a multi-dimensional system is required to describe the spreading flame problem. Notwithstanding much progress over the years, a thorough understanding of solid fuel flame spread is not in hand, with the complexity of the problem partly explaining the research status.

In order to generalize experimental results and to develop simplified theories, the flame spread over solids is traditionally classified into two sub-categories: opposed flow spread when a flame spreads against the oxidizer flow, and concurrent or flow-assisted spread when a flame spreads in the same direction as the oxidizer flow. On the other hand, there exist two limiting cases with regard to the thickness of the solid fuel: thermally thin when the fuel is heated uniformly throughout its entire thickness by the spreading flame, and thermally thick when solid heat conduction fails to penetrate the entire fuel thickness such that significant temperature gradients develop in the normal direction to the surface. The division of flame spread between distinct sub-categories is meaningful in the sense that the dominant mechanisms are different in the model problems, and most studies have fallen into the four regimes.

It is well known that the flame spread behavior in opposed or concurrent flows depends strongly on the magnitude of the flow velocity. The influence of high-velocity and moderate-velocity has been investigated by numerous experimental and theoretical works. For gas velocities smaller than that induced by buoyant flow, however, flame spread experiments have been a challenge. This situation stems from the fact that it is difficult to offer a very small velocity convective flow in normal gravity and a microgravity environment is needed to eliminate the complications of buoyant flow. Particularly, for a thick solid, the ignition and subsequent transition to flame spread has a relatively long time scale, which precludes the use of ground-based facilities such as drop towers for a microgravity test. From the viewpoint of fundamental understanding of flame spread, microgravity environment is of interest to researchers because a purely forced oxidizer flow can be generated and therefore flame behaviors in low-velocity flow regime could be examined. Studies on this type of combustion, however, have been motivated primarily by the practical concerns of fire safety for inhabited spacecraft in the past decades, since spacecrafts are designed to maintain a low velocity atmospheric circulation (of the order of 10 cm/s).

The present article surveys recent experimental results of flame spread and extinction phenomena over solid fuels, which have been obtained by the authors' research team. Since several excellent reviews have addressed the solid flame spread process, this review is prepared with a narrow scope to focus on spreading flames in the low-velocity flow regime, whereas the highlighted topics are of scientific interest and practical importance. Readers are referred to Fernandez-Pello [1], Wichman [2], Sirignano and Schiller [3], and the book by Quintiere [4] for a comprehensive review of the science of flame spread, while readers who desire a review of flame spread in microgravity are referred to T'ien et al. [5] and Fujita [6].

2 Effects of a Confined Space on Microgravity Flame Spread

Most of previous studies on microgravity flame spread have been performed in open areas. A realistic fire could start and develop in constrained spaces [7, 8]. Meanwhile, the available test section sizes for microgravity experiments are usually rather limited, implying that the influence of a confined space should be taken into account to interpret the experimental results. Only few studies have treated geometry effects on flame spread in microgravity [9–11]. Although they demonstrated clearly the modifications of flame characters in a confined space, the problem deserves more effort. In particular, the quantitative effect of a finite size space on opposed-flow flame spread remains to be examined systematically considering the varied space dimensions.

In our study, effects of confined spaces on flame spread over thin solid fuels in a low-speed opposing air flow have been investigated by combined use of microgravity experiments and numerical computations [12]. To examine the effect of a confined space, the flow tunnel had a variable height in a range of 1.5–5 cm (in experiments) or 6 cm (in computations), while the velocity of the imposed flow was fixed at 5 cm/s. Thin cellulosic paper was used as the solid fuel. The microgravity experiments were conducted in the 3.6 s drop tower at the Key Laboratory of Microgravity, CAS, and flame data were gathered for spread rate, flame length, and flame appearance for various tunnel heights. The observations were compared with the numerical results that based on a two-dimensional flame spread model. Simulations also examined the flow field in the tunnels and the heat release rate from the flame. The results were used to explain the observed flame behaviors in confined spaces.

The drop-tower experiments showed that the transition of the opposed-flow flame to a steady-state microgravity flame was completed within approximately 1 s from the drop start. Presented in Fig. 1 are side-view images of the microgravity flames spreading in flow tunnels of different heights. In the most narrow tunnel (tunnel height, H, is 1.5 cm), the visible flame is very small. The brightest part of the flame is at or near the leading edge and the flame is almost entirely faint blue, indicating an absence of significant soot production. As the tunnel height increases slightly to 2 cm, the length and luminance of the flame increase dramatically, with a bright yellow trail visible behind the blue leading edge. Near the trailing edge, the flame becomes dimmer and thinner, and a glow of soot is noted. The overall flame curves away from the fuel plane and then keeps nearly parallel with the fuel plane. When H increases to 2.5 and 3 cm, the overall flame length increases further. However, a more significant change is observed to occur in the trailing portion of the flame, which curves back toward the fuel plane near the trailing edge. In an even higher tunnel ($H = 3.5$ and 4 cm), the flame tail becomes nearly flat again, curving very slightly back towards the fuel plane near the trailing edge. There is evidence that the tunnel height reaches a critical value at approximately 3 cm, beyond which the changes of the flame appearance are gradual and monotonic with increasing tunnel height. In fact, combustion tests have also been carried out in a 1 cm high tunnel. The flame

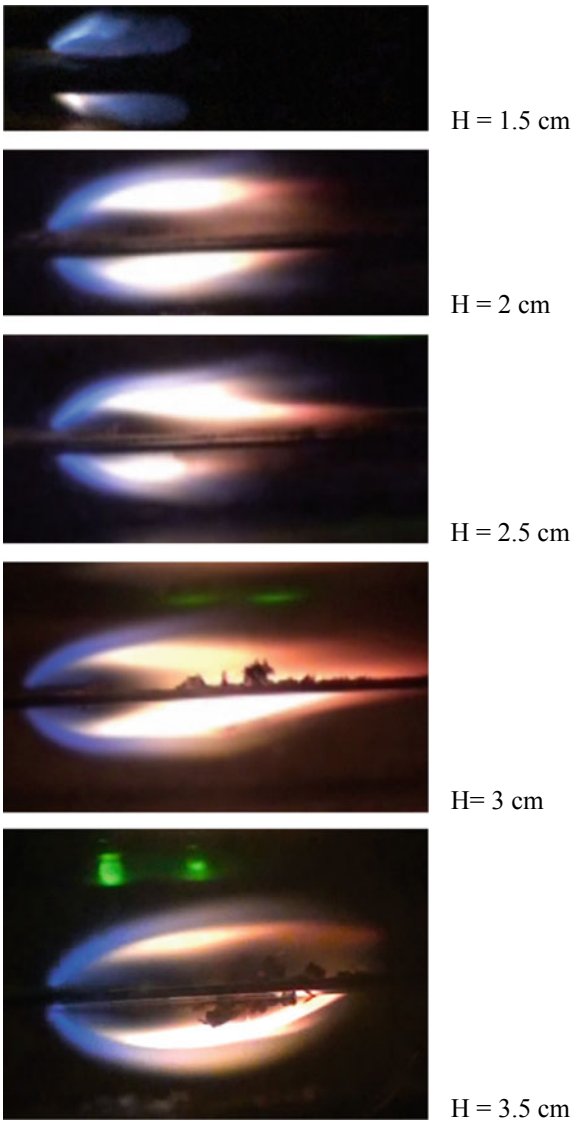

Fig. 1 Images of steady microgravity flames spreading in flow tunnels of different heights. The air flow enters from left at 5 cm/s and 1 atm. (reprinted from reference [12]. Copyright 2015, with permission from Springer Nature)

extinguishes shortly after ignition, and a self-sustained spreading flame could not be achieved in the slow air flow of 5 cm/s under microgravity conditions. In addition to heat loss, such a flame-spread limit may be caused by the limited oxygen supply into the tunnel.

The tunnel size has a significant influence on the magnitude of flame spread rate. It is shown that the spread rate curve is non-monotonic with respect to tunnel height. When H is increased from 1.5 cm, the spread rate increases until a maximum is reached at approximately $H = 3$ cm. The flame spread is 75% faster in the 3 cm tunnel than in the 1.5 cm tunnel (1.325 cm/s as against 0.758 cm/s). A reverse flame spread trend is observed when $H > 3$ cm, i.e. the spread rate decreases with increasing tunnel height. In this regime, an interesting observation is that an invariable spread rate may be approached in a flow tunnel with large height since the spread rate seems to decrease asymptotically with H. Flame spread rates in a 20 cm diameter tunnel have been measured by Olson [13] for a cellulosic paper whose area density is similar to that of the present fuel. In an air flow of 5 cm/s, the spread rate was determined to be 1.08 cm/s, comparable to the present test value of 1.14 cm/s which is obtained at $H = 5$ cm. It implies that the confinement effects on flame spread become less important when the test tunnel is relatively large. Compared with experiments, the computations produce higher spread rates especially in the low range of H. The non-monotonic trend of flame spread rate versus tunnel height, however, is well predicted. The entire flame length curve is also non-monotonic with tunnel height, while a maximum value occurs at approximately $H = 3$ and 4 cm from the experiments and computations, respectively.

Since the flame spread rate depends on heat release rate from the flame [4], the computed result for the total heat release rate is examined as a function of the tunnel height. It is shown that the tunnel size has a significant influence on the chemical energy release. The total heat release rate is highest in the 3 cm high tunnel, and it decreases in narrower or higher tunnels. Thus, a non-monotonic trend of heat release rate vs. tunnel height is obtained. This trend can satisfactorily explain the variation of the flame spread rate with tunnel height, although it should be regarded as a result of the flow modification in confined spaces.

Figure 2 shows the computed flow velocity contours around the spreading flame for five different tunnels. Since there is thermal expansion near the flame and the expansion is constrained in the direction perpendicular to incoming flow (y direction), the streamwise flow (in the x direction) is accelerated towards the downstream region. This flow acceleration effect is observed in all the tunnels studied. But it is most pronounced in intermediate-height tunnels ($H = 3$–4 cm) because the degree of the acceleration depends on both the flame size and the tunnel dimension. Note that the larger downstream velocity produces a longer flame. Thus, the trend of flow acceleration behind the flame is consistent with the non-monotonic variation of flame length with tunnel height. With the velocity component in the y direction, there is an additional observation about the confinement influence. At the leading edge of the flame, the flow is directed outwards due to the blowing of pyrolysis gases from the fuel. Above the flame, however, the flow deflects back from the tunnel wall. This inward flow pushes the flame towards the fuel surface, and transports more oxygen into the flame (compared with the no inward flow case which is assumed to happen in a large tunnel). Because of the enhanced combustion reaction in the flame, the heat flux from the flame to the fuel is increased, so the flame spread becomes faster. Once again, such a flow trend is most pronounced in intermediate-height tunnels, explaining the trend of flame spread rate with tunnel height.

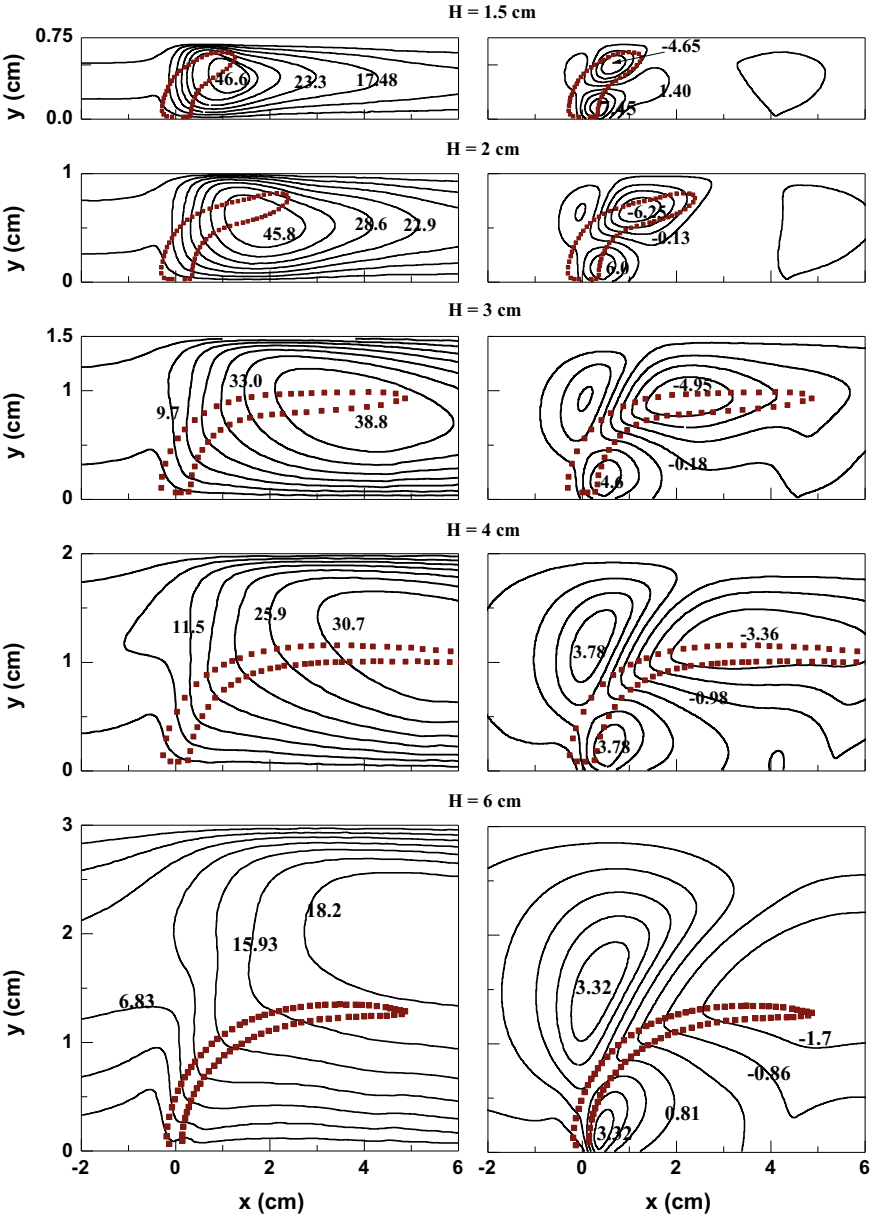

Fig. 2 Flow velocity contours around the flame for different tunnel heights. Left column: velocity component in the streamwise direction (x direction); Right column: velocity component in the direction perpendicular to the incoming flow (y direction). (reprinted from reference [12]. Copyright 2015, with permission from Springer Nature)

3 Near-Limit Instabilities of Concurrent Flame Spread Over Thin Solids

As an alternative mode of solid combustion, smoldering wave shares much common characteristics with spreading flame so far as their structural properties and the involved physical mechanisms are concerned [14]. Followed the experimental studies of smoldering combustion by Olson et al. [15], Zik and Moses [16, 17], and Zik et al. [18], Olson et al. [19] conducted experiments on opposed-flow flame spread over thin solid fuel in actual and simulated (by employing a narrow channel apparatus) microgravity conditions. Similar to the smolder case, the initially continuous flame front was observed to break into separate flamelets when the imposed oxidizer flow velocity was reduced near to the quenching limit, leaving a fingering pattern on the fuel surface. Zhang et al. [20] suggested that diffusive-thermal instability is the mechanism that is responsible for the fingering patterns observed in the flame spread mode. So far the cellular and fingering instabilities identified in experiments, either in smolder or flame spread mode, have been confined to the opposed flow regime. In a numerical study of diffusive-thermal instability of forward smolder waves, Lu and Dong [21] predicted that fingering instability can develop near the quenching limit where heat loss should play a dominant role.

The experimental work of Wang et al. [22], which was partly aimed at providing experimental data in the context of concurrent flame spread, has been inspired by the numerical results of Lu and Dong [21]. The objective of the work was to obtain an overall picture of the dynamical behavior of concurrent flame spread near the quenching limit. In order to suppress buoyant convection, a Narrow Channel Apparatus (NCA) was developed for experimental study of concurrent flame in very slow oxidizer flows. For all of the tests, thin filter paper was used as the solid fuel sample, which had an effective width of 150 mm and a length of 254 mm.

The experimental results show that, when the imposed oxidizer flow velocity is above an oxygen concentration dependent threshold, the flame spread is usually characterized by a continuous flame front and a uniform spread rate, and is therefore deemed to be stable. If the oxidizer flow velocity is reduced below the threshold, the flame front breaks into separate flamelets, thus marking the onset of flame instability. Two distinct types of instabilities are identified, namely, fingering or cellular instability, which is characterized by cellular flame fronts with fingered burned-out pattern trailing behind, and traveling wave instability, which is characterized by transverse creeping motion of the flamelets along the unburned fuel edge. Both types of instabilities are usually accompanied by recurrent flamelet growing and splitting during the flame spread process. A critical oxygen concentration, which is approximately 19% for the fuel tested, is identified as a separation between these two instability regimes. Specifically, for oxygen concentrations below the critical value, the instability is of fingering or cellular type, whereas for supercritical oxygen concentrations traveling wave instability prevails.

Shown in Fig. 3 is a typical evolution process of flame spread that demonstrates fingering or cellular instability. In an atmosphere with oxygen concentration of 15%

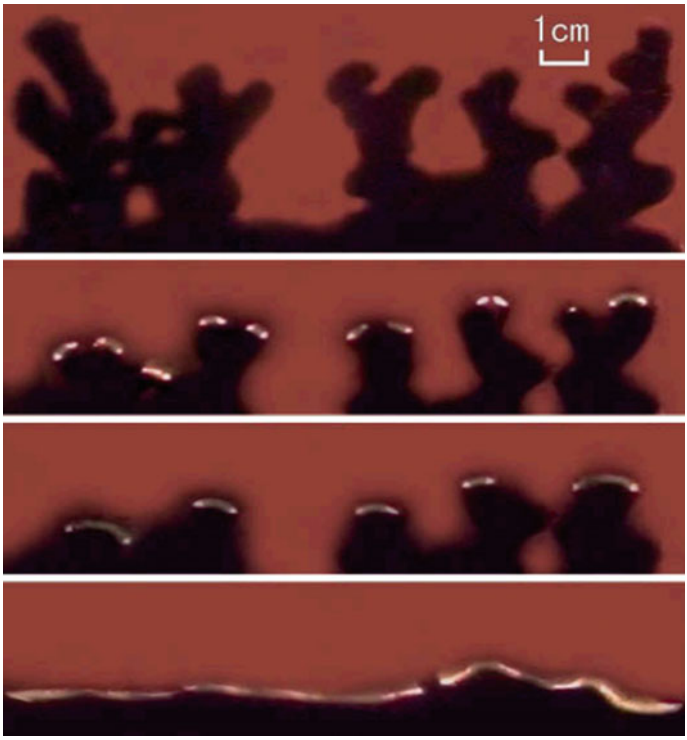

Fig. 3 Flame evolution process demonstrating fingering or cellular instability. (reprinted from reference [22]. Copyright 2016, with permission from Taylor & Francis)

and gas flow velocity 6 cm/s, shortly after ignition, the initially continuous flame front breaks into several discrete flamelets, which spread downwind together and leave behind a fingering burned-out pattern. It is evident that each flamelet assumes an arc shape, with the convex surface facing downstream. Moreover, the arc-shaped flamelet grows in width as it moves forward, and once its width exceeds a critical value, the flamelet splits in the middle into two children flamelets, resulting in a bifurcation of the trailing finger tip. However, all of the second-generation children flamelets go out eventually. A test with an even lower velocity, 5 cm/s, has been carried out subsequently, but it turned out that the initiated flame front failed to spread forward and extinguished soon after ignition. This suggests that the quenching limit for the current oxygen concentration should lie between 5 and 6 cm/s.

When the gas flow velocity is increased to 7 cm/s at the same oxygen concentration (15%), the initially continuous flame front is seen to break into three isolated flamelets, of which only one is survived. Subsequently, this single flamelet undergoes a series of very regular, period-doubling-like bifurcation processes, which are characterized by recurrent flamelet growing and splitting, along with random merging and extinction of the children flamelets. Eventually, the survived children flamelets

succeed in burning through the fuel sample, leaving behind a tree-like burned-out pattern. Such a period-doubling-like bifurcation mode arising in concurrent flame spread is qualitatively reminiscent of the front splitting mode identified in the experiments of reverse smolder [15–18] and opposed flow flame spread [19, 23], although the gas flow directions are opposite in the two situations. This suggests that the currently identified fingering or cellular regime of concurrent flame spread may also be a manifestation of the diffusive-thermal mechanism.

Figure 4 presents a sequence of images for concurrent flames spreading in air (oxygen concentration 21%) with flow velocity 3 cm/s, showing the evolution of typical traveling wave instability. As can be seen, after an initial developing stage, the continuous flame front is survived by a single flamelet. In the subsequent development, this single flamelet experiences recurrent growing and splitting, spawning a train of children flamelets that distribute along the unburned fuel edge. However, different from the fingering or cellular regime, each of the flamelets undergoes an essentially transverse creeping motion, traversing the fuel edge often in a back and forth manner. As a consequence, the unburned fuel maintains a relatively smooth edge at all times and there is no leftover trailing behind the flamelets.

By conducting systematic experiments that cover comprehensive ranges of oxygen concentration and flow velocity, we have plotted the flammability map and stability diagram of concurrent flame spread. As shown in Fig. 5, the flammability boundary exhibits a *U*-shaped curve, with the interior corresponding to the flammable region. This observation is consistent with the computational results of Kumar et al. [24]. The left branch of the flammability boundary corresponds to the quenching limit, near which heat loss plays a significant role in flame spread; the right branch is believed to correspond to the blow-off limit, which, due to the focus of the study (flame behaviors near quenching limit), has not been delineated except for very low oxygen concentrations. The merging point of the two branches defines an absolute oxygen limit, below which concurrent flame spread cannot be sustained for any imposed flow velocities.

The flammable region in Fig. 5 can be divided into three sub-regions, which correspond to distinct flame spread regimes. Specifically, the marginal stability boundary separates a region that is characterized by essentially continuous flame fronts spreading at uniform speeds, from regions where the flames suffer instabilities. The marginal stability boundary lies very close to the quenching limit for higher oxygen concentrations and progressively gets farther as the oxygen concentration goes down towards the absolute oxygen limit. Herein we could come to a conclusion that the flame spread is more susceptible to flame instabilities in low oxygen environments. The second dividing line corresponds to a critical oxygen concentration, which is approximately 19% for the tested fuel. It divides the entire unstable region into two parts: below the critical oxygen concentration, the flame instability is of fingering or cellular type, whereas above the critical oxygen concentration, the flame instability is of traveling wave type.

Wang et al. [22] asserted that the two kinds of instabilities identified in concurrent flame spread are diffusive-thermal in nature and may be classified into the category of near quenching limit instability of non-adiabatic diffusion flames. In addition, an

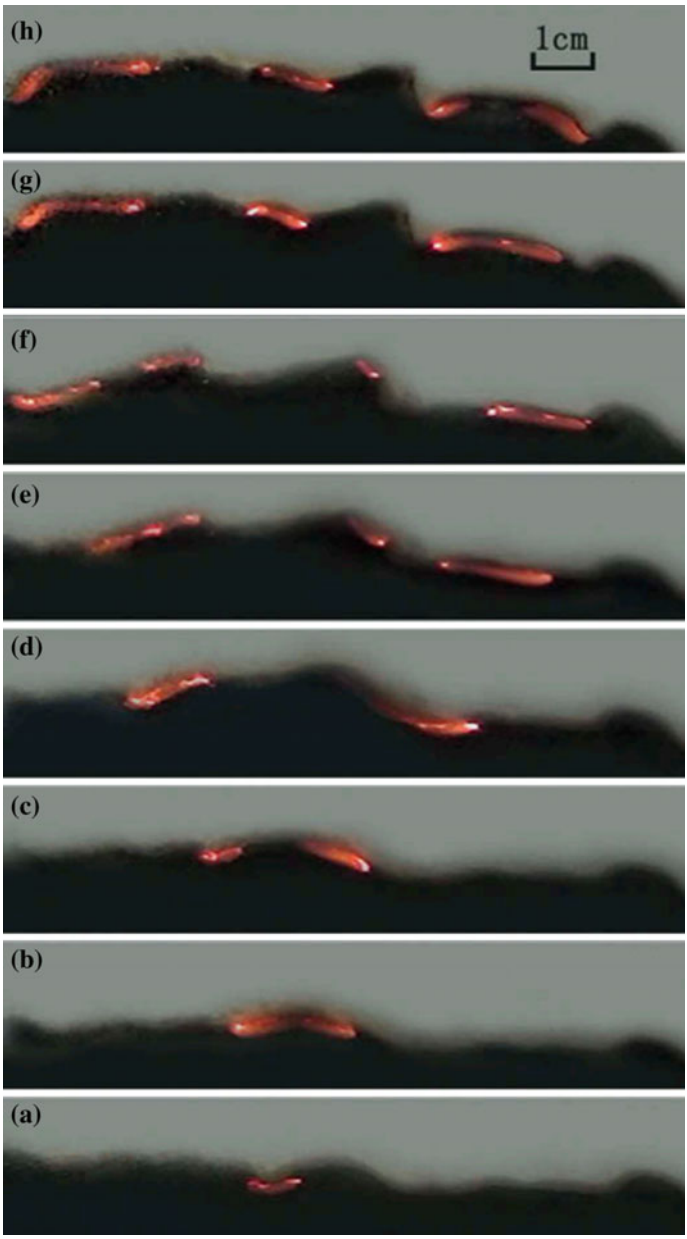

Fig. 4 Flame evolution process demonstrating traveling wave instability. (reprinted from reference [22]. Copyright 2016, with permission from Taylor & Francis)

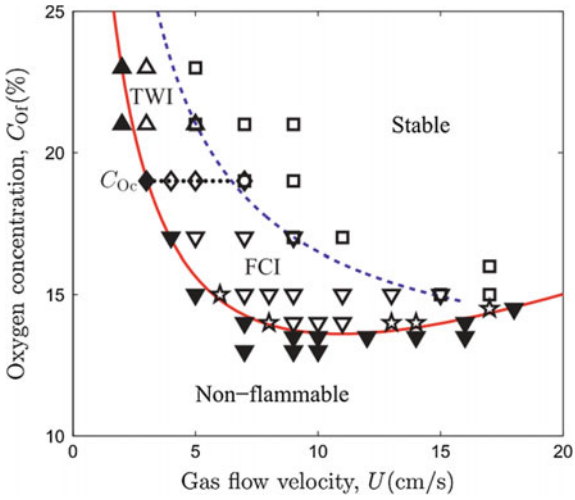

Fig. 5 Flammability map and stability diagram of concurrent flame spread. (reprinted from reference [22]. Copyright 2016, with permission from Taylor & Francis)

attempt had been made to gain insight into the physical mechanisms of the flame instabilities by exploiting the similarities between concurrent flame spread and forward smolder combustion. It was found that the conditions for the onset of fingering instability in flame spread are in accord with the stability analysis results of smolder waves [21].

4 Opposed versus Concurrent Flames Spreading Over a Thick Solid

The forward heat transfer is mainly by gas-phase conduction in opposed-flow flame spread. In contrast, convection prevails for concurrent spread. Since convective heat transfer is usually more effective than conduction, concurrent spread is generally expected to be more rapid and hazardous than opposed spread. As the velocity of the convective oxidizer flow decreases, however, the relative effectiveness of the heat transfer modes may be changed. For thermally-thin fuels, both microgravity experiments and numerical simulations [13, 24–26] have revealed that the opposed flame can spread faster than the concurrent flame if the flow velocity is low enough. Due to constraints on the available test time in drop towers, most research on microgravity flame spread has dealt with thermally-thin fuels [5], and the number of data points has been limited for flames spreading over thick fuels in the low-velocity flow regime. Such that our understanding of the near-limit flame spread over thick fuels is far from mature. The problem requires further research on both opposed and concurrent flame spreads.

By employing a Narrow Channel Apparatus to suppress buoyant flow, Zhu et al. [27] conducted systematical experiments to observe the flame spread and extinction

processes over a thick PMMA sample (with a thickness of 10 mm) in opposed and concurrent flows. The tests focused on low-velocity flow regime ($U \leq 15$ cm/s) and hence complemented experimental data previously reported for high and moderate velocity regimes. The flame spread rates were measured as a function of the velocity and oxygen concentration of the forced gas flow. The experimental results were analyzed in the framework of existing theoretical models of flame spread, and the data for opposed flames were compared with those for concurrent flames. Flammability maps were constructed for both opposed and concurrent flames. A comparison of flammability limits between the two flame spread modes revealed their relative flammability in low-velocity flows.

Flame spread rates are shown in Fig. 6 as a function of flow velocity for both opposed and concurrent flames. In the low-velocity flow regime considered, the flame spread rate increases monotonically as the gas velocity increases in both flame spread modes. In opposed flows, the flame spread rate also depends on oxygen concentration, and it increases with increasing oxygen concentration. In concurrent flows, however, the flame spread rate appears practically independent of the oxygen concentration. A more interesting observation is that, at a given flow velocity, the opposed flame spreads much faster than the concurrent flame, and this trend remains unchanged throughout the flow velocity range in the experiments. In particular, at very low gas velocities (near quenching limits) or at high oxygen concentrations, the spread rate in opposed spread may be one order of magnitude larger than that in concurrent spread. Also plotted in Fig. 6 are the microgravity data on opposing flame spread rate over PMMA plates 20 mm thick, which were measured in sounding rocket experiments by Olson et al. [28] at 50% O_2 and $U = 1, 5$, and 10 cm/s. They are substantially below the NCA results for the same oxygen level, while a similar trend is exhibited as the flow velocity increases. This discordance may be contributed to the fuel sample size adopted in the experiments. In the microgravity tests the sample is rather narrow (6.35 mm). Since lateral heat loss from the flame exerts an influence over a distance of the order of cm in low-velocity flow [11], the flame is cooled

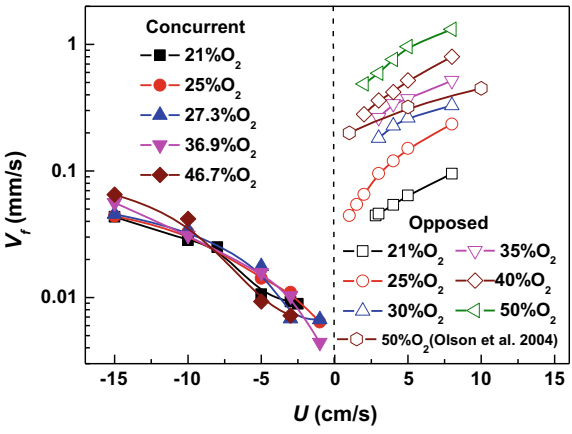

Fig. 6 Flame spread rate as a function of flow velocity for opposed and concurrent spreading flames at different oxygen concentrations. The velocity of opposed flow is defined as positive, and concurrent flow as negative. (reprinted from reference [27]. Copyright 2016, with permission from Springer Nature)

everywhere across its width, resulting in a reduced spread rate. On the contrary, in our experiments the sample has a much larger width (50 mm), and for the center portion of the flame where the spread rate is measured the side heat loss effect can be avoided. Note that the effect of the sample width on flame spread rate measurements has been extensively observed for thin solid fuels [11, 29, 30].

For opposed flame spread in moderate- and high-velocity flow regimes, the flow effects have been shown to be contained a non-dimensional controlling parameter, the Damköhler number [31, 32]. In Fig. 7, the flame spread rate data reported in Fig. 6 for opposed flame are presented versus the Damköhler number of Bhattacharjee et al. [32], Da_{EST}, together with the experimental results of Fernandez-Pello et al. [31] for high flow velocities. Herein the spread rates are normalized with a theoretical spread rate, $V_{f,\mathrm{EST}}$, predicted by an extended simplified theory (EST) of opposed flame spread [32]. The formula for $V_{f,\mathrm{EST}}$, based on EST, overcame the main drawbacks of the de Ris formula [33] and performed significantly better than the latter. However, it is noted that the assumptions of infinitely fast chemistry and neglect of radiation are retained in EST, and such that the derived spread rate formula is for the thermal regime (i.e., flame spread in moderate-velocity flow). In Fig. 7, it is clearly seen that the non-dimensional spread rates, obtained under extensive environmental conditions, collapse onto a universal curve over the entire range of the Damköhler number. The shape of the collapsed curve suggests that three distinct segments may be identified with respect to Da_{EST}. For intermediate Damköhler numbers, $10^5 < Da_{\mathrm{EST}} < 10^6$, $V_f \approx V_{f,\mathrm{EST}}$ ($V_f/V_{f,\mathrm{EST}} \approx 1$), and the flame spread is in the thermal regime; for low $Da_{\mathrm{EST}}(<10^5)$, V_f is depressed below $V_{f,\mathrm{EST}}$ ($V_f/V_{f,\mathrm{EST}} < 1$) by the finite-rate chemical kinetics, and the flame spread is in the kinetic regime; the third regime, characterized by large Da_{EST} ($>10^6$), is indicated by the present experimental data, where the flame spread is in the low-velocity quenching regime and the spread rate is lowered ($V_f/V_{f,\mathrm{EST}} < 1$) primarily by radiative heat loss.

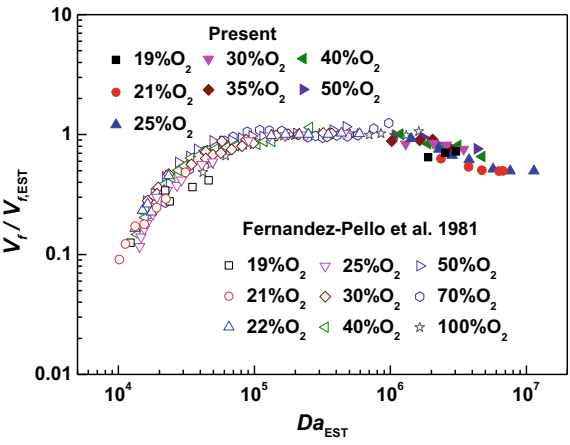

Fig. 7 Correlation of non-dimensional flame spread rate, $V_f/V_{f,\,EST}$, with Damköhler number, Da_{EST}, for opposed flame spread. (reprinted from reference [27]. Copyright 2016, with permission from Springer Nature)

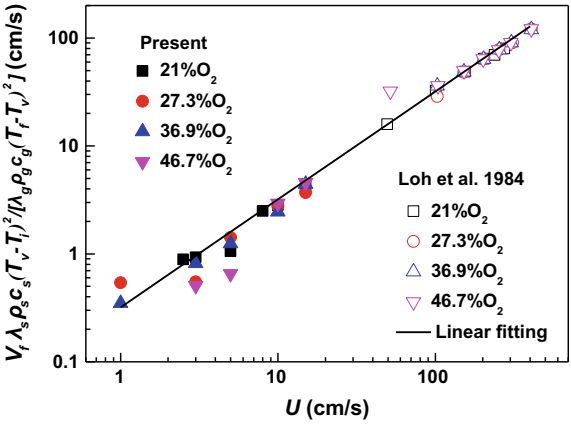

Fig. 8 Experimental spread rate for concurrent spreading flame in a comparison with theoretical prediction. (reprinted from reference [27]. Copyright 2016, with permission from Springer Nature)

For concurrent flame, the theoretical models [1, 34, 35] predicted that the spread rate is linearly proportional to the flow velocity: $V_f\ \lambda_s\rho_s c_s(T_v - T_i)^2/[U\lambda_g\rho_g c_g(T_f - T_v)^2] = \text{const}$. Where T_f is the adiabatic flame temperature, T_v the pyrolysis temperature of the solid, T_i the initial temperature of the solid, λ the conductivity, ρ the density, and c the specific heat, and the subscripts s and g denote the gas and sold phase respectively. In Fig. 8, for concurrent flame, a plot of $V_f\ \lambda_s\rho_s c_s(T_v - T_i)^2/[\lambda_g\rho_g c_g(T_f - T_v)^2]$ is presented versus U for the spread rate data reported in Fig. 6. The experimental data of Loh and Fernandez-Pello [34] for high flow velocities are also given in Fig. 8, and the linear regression line corresponds to their theoretical model. It is seen that the measured flame spread rates agree with the prediction in general, indicating that the heat transfer model captures the controlling mechanisms of flame spread. On the other hand, the experimental results at low flow velocities lie below the model prediction. This deviation may be caused by the neglect of radiative loss in the theoretical model, whereas radiation becomes important in low-intensity flame spread [36].

Using the NCA test results and other published data on opposed flame spread [28, 31], the flammability boundaries for flames over PMMA are plotted for both opposed and concurrent flow configurations (Fig. 9). For the opposed case, the flammability boundary can be obtained over a wide range of flow velocity, showing a typical U-shaped. The left branch of the flammability boundary corresponds to quenching extinction limit in low-velocity flows, and the right branch corresponds to blow-off extinction limit in high-velocity flows. The absolute oxygen limit, indicated by the bottom of the U-shaped curve, is determined to be approximately 18.5% O_2. For the concurrent flame, only a left flammability boundary is shown in Fig. 9 due to the absence of experimental data for high-velocity flows. The absolute oxygen limit for concurrent flame spread is estimated to be around 14% O_2, substantially below that for opposed flame. As can be seen in Fig. 9, the concurrent spread has a wider flammable range than the opposed spread. For concurrent spread, a narrow flammable region is added beyond the flammability boundary of opposed spread. Particularly, when oxygen concentration is reduced below the absolute oxygen limit for opposed spread, a flame can be sustained only in concurrent spread.

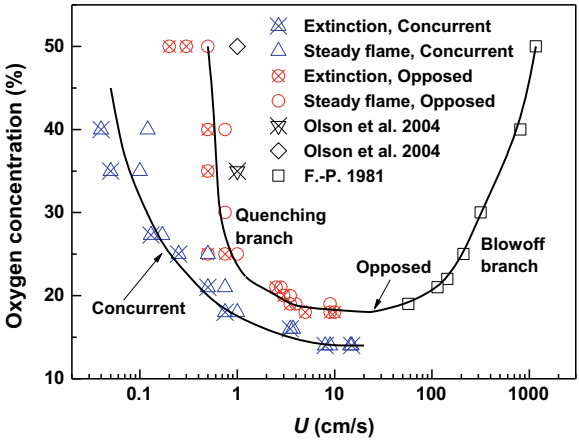

Fig. 9 Flammability boundaries for PMMA in opposed and concurrent flame spread modes (reprinted from reference [27]. Copyright 2016, with permission from Springer Nature)

5 Spread and Dynamic Transition Behaviors of Flames Over a Thick Solid in Microgravity

In this section, some preliminary results of a space-based microgravity experiment, which was conducted aboard the SJ-10 satellite of China in April 2016 to investigate flame spread behaviors over a thermally-thick PMMA in low-velocity flows [37, 38], will be described. We made an observation of flame behaviors in step-changed opposing flows. In other words, the focus was on the spread of steady flames, as well as the flame response to a change of imposed flow.

A payload specifically designed (Fig. 10) have been developed for the space experiment "Ignition and Burning of Solid Materials in Microgravity". The microgravity flame spread experiments are conducted in a 39-L combustion chamber, in which eight flow tunnels are installed. The flow tunnels have an identical cross section of 95 mm × 95 mm and a length of 120 mm, and four of them are used for experiments of flame spread over thick PMMA plate. Each of the four tunnels accommodates an aluminum sample holder. A PMMA sample, with a size of 61.6 mm long × 50 mm wide × 10 mm thick, is mounted flush with the sample holder. Five thermocouples (type-R, 0.075 mm in diameter) are located along the centerline of the sample to measure the gas and solid phase temperatures during the test. A resistively heated wire is used as the igniter, which is embedded in the sample 15.8 mm away from the downstream edge. Such a design, igniting at the middle of the sample, is intended to observe a potential combination of opposed and concurrent flame spreads, although previous studies have focused primarily on either opposed or concurrent flame. Under the tested conditions, however, opposed-flow flame spread occurred merely. The forced gas flow in the tunnel is induced by a fan fixed at the downstream end of the tunnel. The bulk flow velocity is calibrated using a Laser Doppler Velocimeter (LDV) on ground, and can be adjusted in a range of 0–12 cm/s. At the upstream end of the channel, an aluminum honeycomb is installed

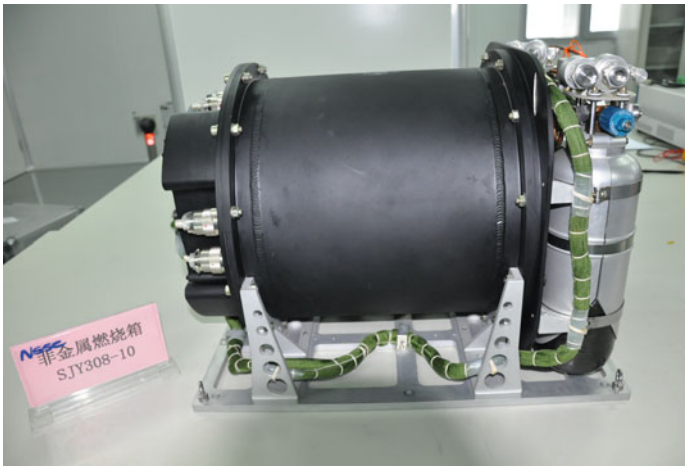

Fig. 10 Flight hardware of the microgravity experiment aboard the SJ-10 satellite

Fig. 11 Cross-sectional view of one flow tunnel

to straighten the flow. On two orthogonal walls of the flow tunnel, observation windows are presented. Shown in Fig. 11 is the cross-sectional view of one flow tunnel, thereby the test section configuration is demonstrated.

In order to establish the specified oxidizer atmosphere in the combustion chamber, a gas control system is integrated with the payload. The gases are filled into the chamber from two bottles, which are charged with 21 and 50% O_2–N_2 mixtures, respectively. At the beginning of each test, residual gas in the chamber is vented to the vacuum of outer space, and then gases from the bottles are charged into the chamber one after the other according to a specified pressure ratio. By blending the two mixtures, the desired O_2–N_2 mixture with preset oxygen concentration is

Table 1 Prescribed time durations of gas flow velocities in each experiment

Oxygen concentration \ Gas flow speed (Time)	9 cm/s	6 cm/s	3 cm/s	0
40%	60 s	50 s	150 s	> 15 min
35%	55 s	40 s	90 s	> 15 min
30%	80 s	80 s	120 s	> 15 min
25%	90 s	90 s	150 s	> 15 min

achieved in the chamber. The chamber pressure is monitored by a pressure transducer. The oxygen concentration is measured by an oxygen transducer in real time. Oxygen concentrations specified for the four flame spread tests are 25%, 30%, 35%, and 40%, respectively, whereas the pressure is at 101 kPa. The microgravity experiments are performed one by one during the orbital flight mission. The experimental procedure is automatically controlled. Firstly, an initial flow with a velocity of 9 cm/s is established in the tunnel. The igniter is then energized for 20 s. In the subsequent duration, the gas flow is adjusted three times with a step change, decreasing to 6 cm/s, 3 cm/s, and finally to 0. Each flow velocity is kept for a prescribed period as listed in Table 1. The flame spread process is simultaneously recorded by two color CCD cameras at a framing rate of 25 fps from top view and side view.

Figure 12 shows the opposed-flow flame spread processes when the flow undergoes stepped changes from 9 to 3 cm/s at 40%, 35%, and 30% O_2, respectively. Depending on the ambient oxygen concentration, the flame initially established over the fuel takes two different forms. At 40 and 35% O_2, it appears as a uniform flame, which extends across the sample width with a continuous leading front; at 30% O_2, a small, three-dimensional flame is achieved, which is named flamelet. As the flow velocity is decreased from 9 to 6 cm/s at 40 and 35% O_2, the flame front remains continuous after a rapid transition process. When the flow is further reduced to 3 cm/s in either oxygen atmospheres, the uniform flame changes its apparent form into flamelets after a relatively long transition process, noting that two separated flamelets forms at 40% O_2 and a single flamelet at 35% O_2. The flamelets go to extinction when the flow is stopped finally and thus a quiescent environment is achieved. At 30% O_2 the initial flamelet survives as the flow decreases from 9 to 6 cm/s, and the transition process is rather short. But it extinguishes when the flow decreases to 3 cm/s. The observed flame spread modes are summarized in Table 2. In the 25% O_2 test, the flame is observed to fail to spread following the ignition transition.

It is seen in Fig. 12 that the flame can respond to the sudden step change of the gas flow velocity to re-establish a new steady state. The transition process between two similar flame modes is relatively short. The transition from a uniform flame to flamelets, however, lasts much longer, and the transition process is characterized by flame oscillations. Figure 13 gives a flame image sequence showing one cycle of the flame oscillation when the flow is reduced from 6 to 3 cm/s at 40% O_2. First a uniform flame shrinks into individual flames separated by non-burning fuel, and

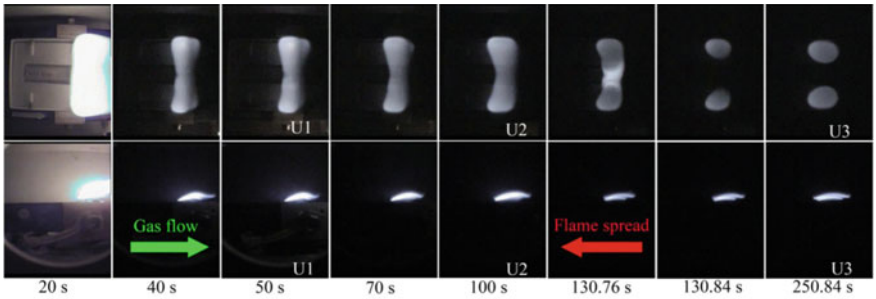

(a) 40% O_2

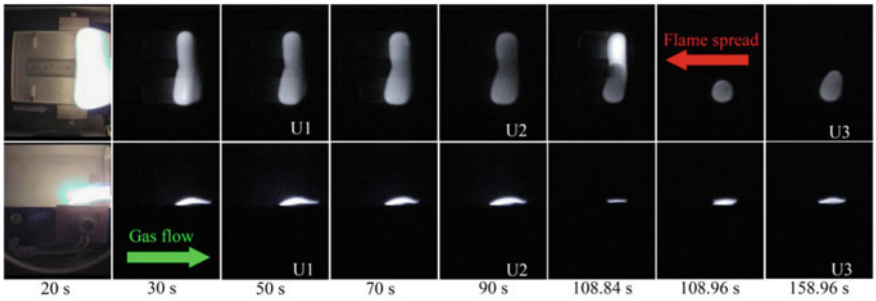

(b) 35% O_2

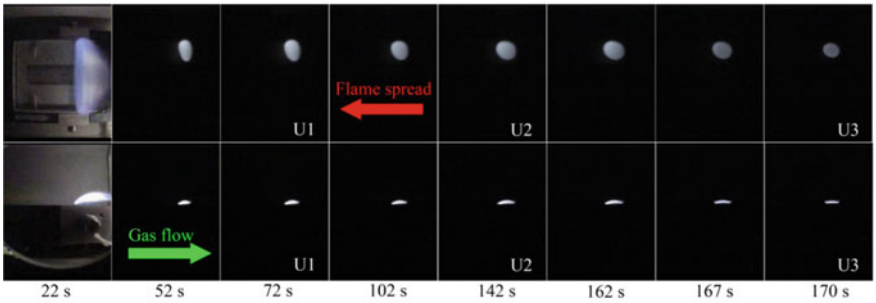

(c) 30% O_2

Fig. 12 Flame spread process after the igniter is turned off at 40%, 35%, and 30% O_2 respectively. U1 = 9 cm/s, U2 = 6 cm/s, and U3 = 3 cm/s. Time is from the moment the igniter is energized

Table 2 Flame spread modes at different oxygen concentrations and flow velocities

Gas flow speed / Flame mode / Oxygen concentration	9 cm/s	6 cm/s	3 cm/s	0
40%	Uniform flame	Uniform flame	Two flamelets	Extinction
35%	Uniform flame	Uniform flame	One flamelet	Extinction
30%	One flamelet	One flamelet	Extinction	\
25%	Fail to spread	\	\	\

Fig. 13 Sequence of front-view images of flame oscillations during flamelets formation at an oxygen concentration of 40% after the flow speed is decreased from 6 to 3 cm/s. The images are separated by an equal time interval 0.08 s

then the flamelets re-connect to form a united flame. This process persisted for about 40 s, and finally spreading flamelets are formed. At 35% O_2, flame oscillations are also observed as the flow velocity is decreased to 3 cm/s, whereas only one flamelet is formed after the transition process. Flame oscillations are also observed when the flamelets go to extinction following sudden decrease of flow velocity. Figure 14 illustrates the dynamic process of flame extinction at 40%, 35%, and 30% O_2. Note that the transition process lasts about 1 s, much shorter than the uniform to flamelets transition.

In Fig. 15, the variations of flame (or flamelet) leading edge position and flame length are shown as a function of time for different oxygen concentrations. As can be seen, except the transition process following the step change of flow velocity, the relative flame position data show a linear variation with time, indicating a constant flame spread rate; but the flame length continually increases with time even at specified oxygen concentration and flow velocity, indicating that the flame does not reach a completely steady state. The leading edge standoff distances are also determined. A constant value can be obtained under a specified oxygen and flow condition after the transition process. The spreading flames after the transition could be regarded as steady because opposed flame spread is controlled primarily by processes in the vicinity of the flame leading edge.

The RGB two-color pyrometry method [39–42] is utilized to resolve the temperature field of the spreading flames. Based on the flame leading edge temperature determined, we carry out an energy balance analysis at the fuel surface:

$$\lambda_g \frac{dT_g}{dy} = \lambda_s \frac{dT_s}{dy} + \dot{m}'' L_v + \varepsilon \sigma T_s^4 \tag{1}$$

where, λ_g, λ_s, ε, T_g, T_s, L_v, σ, and $\dot{m}''$ are gas thermal conductivity, solid phase thermal conductivity, the radiative emittance of the fuel surface, the temperature of the gas and solid, latent heat of vaporization, Stefan-Boltzmann constant and mass burning rate, respectively. The left hand term of Eq. (1) is the conductive heat flux from the flame to the surface. As the energy input at the surface, it does not include the radiative feedback from the flame because this feedback may be ignored for near-limit flames [28]. The three terms on the right hand of Eq. (1) constitute the output of the energy, and they represent the in-depth conduction into the solid, the heat to vaporize the fuel, and the surface radiative heat loss, respectively. The values of each

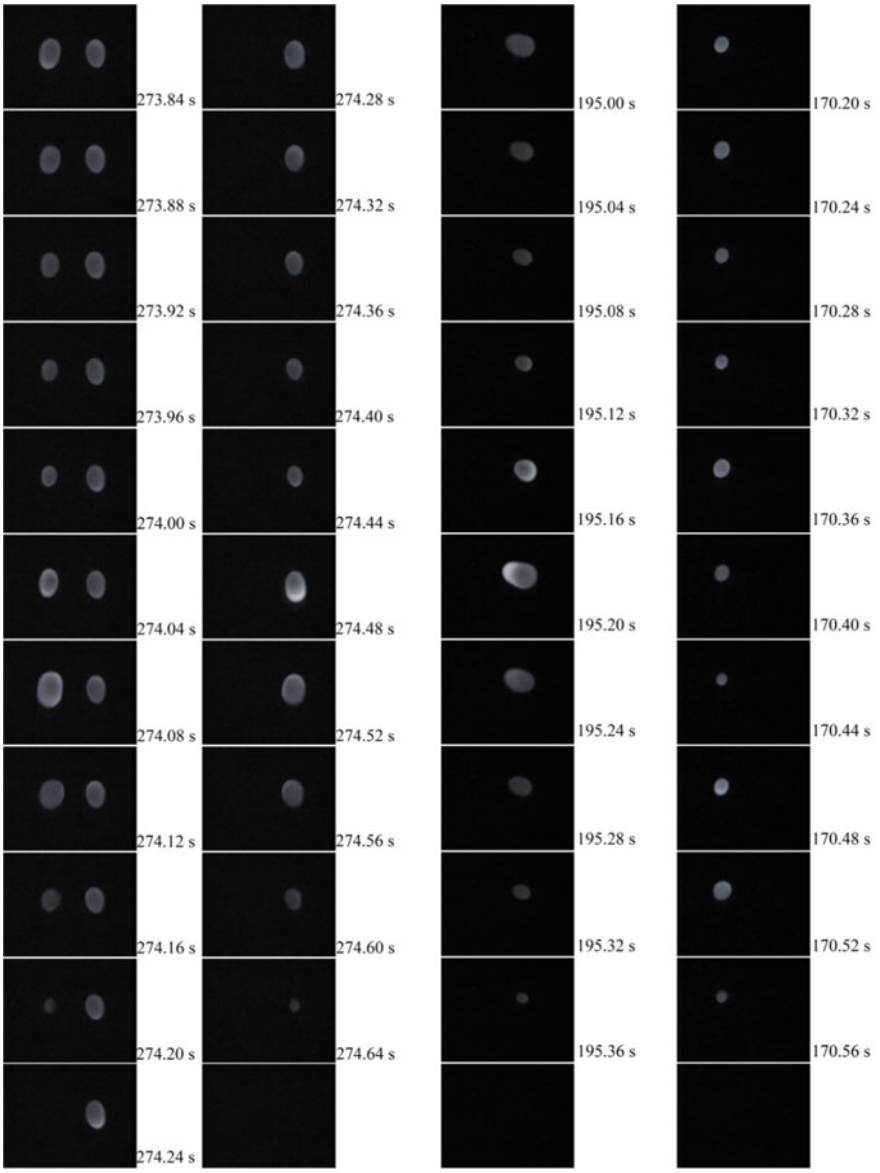

Fig. 14 Sequence of front-view images of flame variation process before extinction. At 40% and 35% O_2, flame spreads in the quiescent environment before extinction, while at 30% O_2, flame extinguishes with a flow speed of 3 cm/s

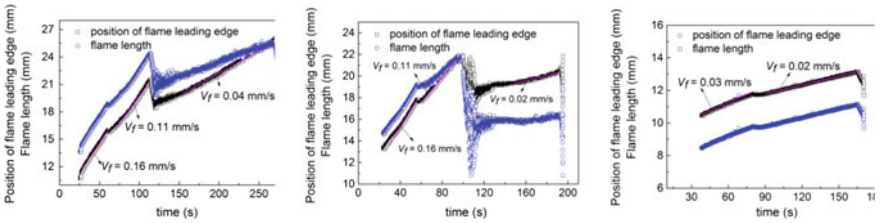

Fig. 15 Relative positions of flame leading edge and flame lengths as a function of time at different oxygen concentrations

heat flux term in Eq. (1) are calculated for flames at different oxygen concentrations and flow velocities. The results are shown in Fig. 16 as a function of flame spread rate. The conductive heat from the flame is clearly seen to decrease with decreasing flame spread rate, resulting from the reduced flame temperature and increased flame standoff distance. The heat loss through solid phase conduction exhibits a similar trend, whereas the surface radiative heat loss remains essentially unchanged. As a result, the heat absorbed by the solid fuel for vaporization, which can be regarded as the net heat flux utilized for flame spread, is observed to decrease as the flame spread slows down. We proceed to examine the heat utilization ratio and the heat loss ratio:

$$F_{utilization} = [\dot{m}'' L_v] \Big/ \left[\lambda_g \frac{dT_g}{dy}\right] \tag{2}$$

$$F_{loss} = \left[\lambda_s \frac{dT_s}{dy} + \varepsilon\sigma T_s^4\right] \Big/ \left[\lambda_g \frac{dT_g}{dy}\right] \tag{3}$$

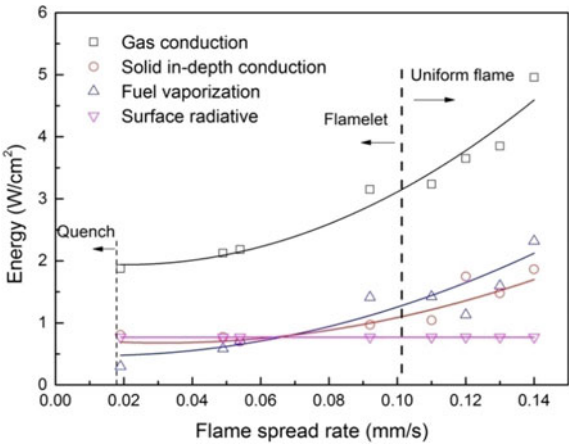

Fig. 16 Heat flux terms in Eq. (1) as a function of flame spread rate

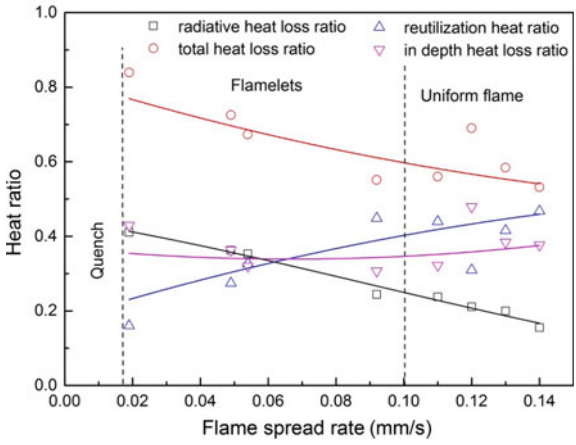

Fig. 17 Heat loss and reutilization ratios as a function of flame spread rate

The ratios are plotted in Fig. 17 as a function of flame spread rate. Overall, the total heat loss ratio increases with the reduced flame spread rate, while the reutilization ratio has an opposite variation trend. At the boundary between uniform flame and flamelets, the loss ratio is about 55%. For flamelets with an extremely low spread rate at extinction, the loss ratio exceeds 80%, which is in accordance with the finding of Olson et al. [28].

6 Summary

The problem of flame spread over solid materials in low-velocity flow regime is of fundamental interest and practical importance for spacecraft fire safety. To test this type of flame spread, a microgravity environment is desired to eliminate the complications of buoyant flow. For thermally-thick solids, long-duration microgravity experiments in space are particularly needed, while the opportunity to conduct space-based experiments has been scarce. In view of these constraints, the Narrow Channel Apparatus (NCA) has been developed to suppress buoyant flow in normal gravity, and thus provide a feasible method for flame spread experiments in slow gas flows.

The present article surveys the major research works that have been recently performed at the Key Laboratory of Microgravity, CAS, to study flame spread in low-velocity flows. The topics involve the confinement effects on flame spread, concurrent flame behaviors near the quenching limit, flame spread and extinction over thick solids in opposed and concurrent flows, and dynamics of spreading flame over thick solids in step-changed flow. The experimental results described herein are obtained from normal gravity NCA tests, microgravity free drops, and space experiments aboard the SJ-10 satellite of China.

Effects of a confined space on flame spread over thin solid fuels in a low-speed opposing air flow is examined by combined use of drop-tower experiments and numerical computations. Results show that the height of the flow tunnel has significant influence on flame behaviors in the low flow velocity regime. The flame spread rate curve is non-monotonic with respect to tunnel height, with the fastest flame occurring in the 3 cm high tunnel. The flame length and the total heat release rate from the flame also change with tunnel height, and a faster flame has a larger length and a higher heat release rate. A confined space is observed to modify the flow around the spreading flame. The flow accelerates in the streamwise direction. Above the flame, the flow deflects back from the tunnel wall. This inward flow pushes the flame towards the fuel surface, and increases oxygen transport to the flame. The flow modification the changes heat release rate of the flame and explains the variations of spread rate and flame length with tunnel height. The results suggest the confinement effects should be taken into account to assess accurately the fire hazard aboard spacecraft.

Flame instabilities near the low flow velocity quenching limit of concurrent flame spread over a thin fuel are experimentally studied by employing a narrow channel apparatus. Depending on the magnitude of the ambient oxygen content and/or the imposed flow, we identify two distinct kinds of instabilities, namely fingering or cellular instability, and traveling wave instability. The former is characterized by cellular flame fronts, and the later by transverse motion of flamelets along the unburned fuel edge. The flammability map and stability diagram of concurrent flame spread are constructed using oxygen concentration and flow velocity as coordinates. The flammable region is divided into three sub-regions that correspond to different flame spread regimes. The marginal stability boundary separates a region where continuous flame spreads from regions where the flames suffer instabilities. Meanwhile, a critical oxygen concentration (approximately 19% O_2 for the tested fuel) divides the entire unstable region into fingering instability and traveling wave instability. It is believed that that the two kinds of instabilities in concurrent flame spread are diffusive-thermal in nature. The physical mechanisms of the flame instabilities may be revealed by exploiting the similarities between concurrent flame spread and forward smolder combustion.

Systematical experiments in a narrow channel apparatus are performed for flame spread and extinction phenomena over a thick PMMA, with emphasis placed on a comparison of the two flame spread modes in low-velocity flows. At a given flow velocity, it is found that the opposed flame spreads much faster than the concurrent one. In general, the spread rate data for both opposed and concurrent flames can be correlated by corresponding prediction models. However, the experimental results in low-velocity gas flows are observed to deviate from theoretical predictions due to the neglect of radiative heat loss in the theoretical models. Flammability limits are presented for both flame spread configurations, showing that concurrent spread has a wider flammable region than opposed spread. An additional flammable area for concurrent spread exists beyond the flammability boundary of opposed spread. Particularly, the oxygen concentration limit for concurrent flame spread is approximately 14% O_2, much lower than that for opposed flame spread (18.5% O_2). It should

be noted that more microgravity experiments are needed to validate the NCA test results.

For a thick solid (PMMA), steady spread, extinction, and dynamic transition behaviors of spreading flame in step changed low-speed opposing flows are investigated by conducting microgravity experiments aboard the SJ-10 satellite. Depending on the oxygen concentration and flow velocity, the spreading flames are observed to take two different forms: uniform flame, and flamelets. A uniform flame sustains at high oxygen concentration. At lower oxygen concentration and flow velocity, however, only flamelets can survive. It is noted that the uniform flame and flamelets can respond to the sudden step change of the gas flow to re-establish a new steady state. The transition process between two similar flame modes, i.e., from uniform flame to uniform flame, or from flamelets to flamelets, is relatively short. By contrast, the transition process from a uniform flame to flamelets lasts much longer, which is characterized by flame oscillations. An energy balance analysis at the fuel surface shows that the heat absorbed by the solid fuel for vaporization decrease as the flame spread rate slows down. The total heat loss ratio increases with decreasing flame spread rate, and excessive heat loss results in the flame extinction ultimately.

Acknowledgements The present works are supported by the National Natural Science Foundation of China (grant No. U1738117) and the Strategic Priority Research Program on Space Science of CAS (grant Nos. XDA04020410, XDA04020202-10). The authors would like to thank all cooperators for their contribution to these studies. Special gratitude is due to Prof. Wen-Rui Hu for his persistent support of the first author's research work.

References

1. Fernandez-Pello AC (1984) Flame spread modeling. Combust Sci Technol 39:119–134
2. Wichman IS (1992) Theory of opposed-flow flame spread. Prog Energy Combust Sci 18:553–593
3. Sirignano WA, Schiller DN (1997) Mechanisms of flame spread across condensed-phase fuels. In: Dryer FL, Sawyer RF (eds) Physical aspects of combustion, a Tribute to Irvin Glassman, Gordon and Breach, pp 353–407
4. Quintiere JG (2006) Fundamentals of fire phenomena. Wiley, Chichester, West Sussex, England
5. T'ien JS, Shih HY, Jiang CB, Ross HD, Miller FJ, Fernandez-Pello AC, Torero JL, Walther D (2001) Mechanisms of flame spread and smolder wave propagation. In: Ross HD (ed) Microgravity combustion: fire in free fall. Academic Press, San Diego, pp 299–418
6. Fujita O (2015) Solid combustion research in microgravity as a basis of fire safety in space. Proc Combust Inst 35:2487–2502
7. Friedman R (1994) Risks and issues in fire safety on the space station. NASA TM-106430
8. Friedman R (2000) Testing and selection of fire-resistant materials for spacecraft use. NASA TM-209773
9. Shih H-Y, T'ien JS (1997) Modeling wall influence on solid-fuel flame spread in a flow tunnel. AIAA paper 97-0236
10. Nakamura Y, Kashiwagi T, McGrattan KB, Baum HR (2002) Enclosure effects on flame spread over solid fuels in microgravity. Combust Flame 130:307–321
11. Zhang X, Yu Y (2011) Experimental studies on the three-dimensional effects of opposed-flow flame spread over thin solid materials. Combust Flame 158:1193–1200

12. Wang SF, Hu J, Xiao Y, Ren T, Zhu F (2015) Opposed-flow flame spread over solid fuels in microgravity: the effect of confined spaces. Microgravity Sci Technol 27:329–336
13. Olson SL (1991) Mechanisms of microgravity flame spread over a thin solid fuel: oxygen and opposed flow effects. Combust Sci Technol 76:233–249
14. Ohki Y, Tsugé S (1974) On flame spreading over a polymer surface. Combust Sci Technol 9:1–12
15. Olson SL, Baum HR, Kashiwagi T (1998) Finger-like smoldering over thin cellulosic sheets in microgravity. Proc Combust Inst 27:2525–2533
16. Zik O, Moses E (1998) Fingering instability in solid fuel combustion: the characteristic scales of the developed state. Proc Combust Inst 27:2815–2820
17. Zik O, Moses E (1999) Fingering instability in combustion: an extended view. Phys Rev E 60:518–531
18. Zik O, Olami Z, Moses E (1998) Fingering instability in combustion. Phys Rev Lett 81:3868–3871
19. Olson SL, Miller FJ, Jahangirian S, Wichman IS (2009) Flame spread over thin fuels in actual and simulated microgravity conditions. Combust Flame 156:1214–1226
20. Zhang Y, Ronney PD, Roegner EV, Greenberg JB (1992) Lewis number effects on flame spreading over thin solid fuels. Combust Flame 90:71–83
21. Lu Z, Dong Y (2011) Fingering instability in forward smolder combustion. Combust Theor Model 15:795–815
22. Wang SF, Wang SD, Zhu KC, Xiao Y, Lu ZB (2016) Near limit instabilities of concurrent flame spread over thin solid fuel. Combust Sci Technol 188:451–471
23. Olson SL, Miller FJ, Wichman IS (2006) Characterizing fingering flamelets using the logistic model. Combust Theor Model 10:323–347
24. Kumar A, Shih HY, T'ien JS (2003) A comparison of extinction limits and spreading rates in opposed and concurrent spreading flames over thin solids. Combust Flame 132:667–677
25. Olson SL, Kashiwagi T, Fujita O, Kikuchi M, Ito K (2001) Experimental observations of spot radiative ignition and subsequent three-dimensional flame spread over thin cellulose fuels. Combust Flame 125:852–864
26. Kashiwagi T, McGrattan KB, Olson SL, Fujita O, Kikuchi M, Ito K (1996) Effects of slow wind on localized radiative ignition and transition to flame spread in microgravity. Proc Combust Inst 26:1345–1352
27. Zhu F, Lu ZB, Wang SF (2016) Flame spread and extinction over a thick solid fuel in low-velocity opposed and concurrent flows. Microgravity Sci Technol 28:87–94
28. Olson SL, Hegde U, Bhattacharjee S, Deering JL, Tang L, Altenkirch RA (2004) Sounding rocket microgravity experiments elucidating diffusive and radiative transport effects on flame spread over thermally thick solids. Combust Sci Technol 176:557–584
29. Altenkirch RA, Eichhorn R, Shang PC (1980) Buoyancy effects on flames spreading down thermally thin fuels. Combust Flame 37:71–83
30. Shih HY, T'ien JS (2003) A three-dimensional model of steady flame spread over a thin solid in low-speed concurrent flows. Combust Theory Model 7:677–704
31. Fernandez-Pello AC, Ray SR, Glassman I (1981) Flame spread in an opposed forced flow: the effect of ambient oxygen concentration. Proc Combust Inst 18:579–589
32. Bhattacharjee S, West J, Altenkirch RA (1996) Determination of the spread rate in opposed-flow flame spread over thick solid fuels in the thermal regime. Proc Combust Inst 26:1477–1485
33. de Ris JN (1969) Spread of a laminar diffusion flame. Proc Combust Inst 12:241–252
34. Loh HT, Fernandez-Pello AC (1984) A study of the controlling mechanisms of flow assisted flame spread. Proc Combust Inst 20:1575–1582
35. Fernandez-Pello AC (1979) Flame spread in a forward forced flow. Combust Flame 36:63–78
36. Zhao XY, T'ien JS (2015) A three-dimensional transient model for flame growth and extinction in concurrent flows. Combust Flame 162:1829–1839
37. Hu WR, Zhao JF, Long M, Zhang XW, Liu QS, Hou MY, Kang Q, Wang YR, Xu SH, Kong WJ, Zhang H, Wang SF, Sun YQ, Hang HY, Huang YP, Cai WM, Zhao Y, Dai JW, Zheng HQ, Duan EK, Wang JF (2014) Space program SJ-10 of microgravity research. Microgravity Sci Technol 26:159–169

38. Zhao HG, Qiu JW, Tang BC, Kang Q, Hu WR (2016) The SJ-10 recoverable microgravity satellite of China. J Space Explor 4(3):101/1–9
39. Shimoda M, Sugano A, Kimura T, Watanabe Y, Ishiyama K (1990) Prediction method of unburnt carbon for coal fired utility boiler using image processing technique of combustion flame. IEEE Trans Energy Convers 5:640–645
40. Lou C, Zhou HC, Yu PF, Jiang ZW (2007) Measurements of the flame emissivity and radiative properties of particulate medium in pulverized-coal-fired boiler furnaces by image processing of visible radiation. Proc Combust Inst 31:2771–2778
41. Hossain MM, Lu G, Yan Y (2012) Measurement of flame temperature distribution using optical tomographic and two-color pyrometric techniques. In: IEEE international instrumentation and measurement technology conference proceedings. IEEE, Graz, Austria
42. Müller B, Renz U (2001) Development of a fast fiber-optic two-color pyrometer for the temperature measurement of surfaces with varying emissivities. Rev Sci Instrum 72:3366–3374